The Meteoritical Society

Meteoritics & Planetary Science 42, Nr 3, 373–385 (2007)
Abstract available online at http://meteoritics.org

Evidence for lithium and boron from star-forming regions implanted in presolar SiC grains

I. C. LYON*, J. M. TIZARD, and T. HENKEL

The University of Manchester, School of Earth, Atmospheric and Environmental Sciences, Oxford Road, Manchester M13 9PL, UK
*Corresponding author. E-mail: Ian.Lyon@manchester.ac.uk

(Received 07 April 2006; revision accepted 03 January 2007)

Abstract–We report the first measurements of lithium and boron isotope ratios and abundances measured in "gently separated" presolar SiC grains. Almost all analyses of presolar SiC grains since their first isolation in 1987 have been obtained from grains that were separated from their host meteorite by harsh acid dissolution. We recently reported a new method of "gently" separating the grains from meteorites by using freeze-thaw disaggregation, size, and density separation to retain any nonrefractory coatings or alteration to the surfaces of the grains that have been acquired in interstellar space. Nonrefractory coats or amorphized surfaces will almost certainly be removed or altered by the traditional acid separation procedure. High Li/Si and B/Si ratios of up to ~10^{-2} were found implanted in the outer 0.5 μm of the grains dropping to ~10^{-5} in the core of the grains. ^{7}Li/^{6}Li and ^{11}B/^{10}B ratios indistinguishable from solar system average values were found. Analyses obtained from SiC grains from the acid dissolution technique showed isotope ratios that were the same as those of gently separated grains, but depth profiles that were different. These results are interpreted as evidence of implantation of high velocity (1200–1800 km s^{-1}) Li and B ions into the grains by shock waves as the grains traveled through star-forming regions some time after their condensation in the outflow of an AGB star that was their progenitor. The results are in line with spectroscopic measurements of Li and B isotope ratios in star-forming regions and may be used to infer abundances and isotopic sources in these regions.

INTRODUCTION

Presolar grains were first isolated from meteorites by Lewis et al. (1987) by dissolving up the meteorite matrix with harsh acids to leave refractory minerals: diamond, silicon carbide, corundum, graphite, and others (Amari et al. 1994; Bernatowicz et al. 1987; Nittler et al. 1997). The grains are condensates from AGB and RGB stars, novae, and supernovae, and the study of their isotopic composition is now a primary driver in modeling these extreme environments (Bernatowicz and Zinner 1997; Clayton and Nittler 2004; Zinner 1998). Oxide layers and amorphous coatings have been observed on some presolar SiC grains (Bernatowicz et al. 2003; Hoppe et al. 1996) and it has recently become clear that the extraction process alters the surfaces of the grains (Henkel et al. 2002; Nittler and Alexander 2003). Any nonrefractory coating, formed either in the star-forming region, the interstellar medium (ISM) or early solar system is certainly lost during the acid extraction. Amorphization of grain surfaces by sputtering or implantation of atoms in the ISM may also make the surfaces vulnerable to etching or removal during the harsh acid extraction. This realization led to efforts to isolate presolar grains from meteorites without using harsh chemicals (Bernatowicz et al. 2003). We developed a "gentle separation" method (Tizard et al. 2005) that yielded presolar grains with their history from star-forming regions and the ISM preserved. This process involved freeze-thaw disaggregation of the matrix from the Murchison meteorite until it was fully decomposed into its constituent micron-size mineral grains. Repeated size and density separation enriched the SiC grain population in a selected fraction up to ~1% and then electron probe microanalysis (EPMA) mapping could be used to identify SiC grains from a residue of grains dispersed on a pure gold surface.

In this study, we concentrate on analyzing Li and B isotope ratios and abundances in both acid residue presolar SiC grains and gently separated presolar SiC grains. We anticipated that Li and B analyses from these grains might be able to shed some light on the sources of materials going into the early solar system, as Li, Be, and B have very low in abundance in the universe compared to other light elements

© The Meteoritical Society, 2007. Printed in USA.

(Anders and Grevesse 1989). Much of the observed abundance of ^{6}Li, Be, and B is thought to be generated by spallation of heavier nuclei producing ^{7}Li/^{6}Li ≈ ^{11}B/^{10}B ≈ 2.5 (Meneguzzi et al. 1971), although much of the existing ^{7}Li abundance is thought to be primordial from Big Bang nucleosynthesis. These elements are also easily destroyed by high-temperature reactions in stars, so ^{7}Li/^{6}Li and ^{11}B/^{10}B ratios from different extraterrestrial environments might be expected to vary greatly. However, this is generally not the case. There is remarkable uniformity between measured isotope ratios of ^{7}Li/^{6}Li ≈ 12 and ^{11}B/^{10}B ≈ 4 in the planets (e.g., Tomascak 2004), meteorites (e.g., Chaussidon and Robert 1998; Chaussidon et al. 1998), presolar grains (Hoppe et al. 2001; Huss et al. 1997), and from spectroscopic measurements of many star-forming regions (Federman et al. 1996; Knauth et al. 2003). We wished to test whether the Li and B isotope ratios and abundances in both acid residue presolar SiC grains and gently separated grains might retain evidence of Li and B from the nucleosynthetic environments where the grains formed or from regions that they passed through on their way into the early solar system. Be was not able to be studied here as it was of lower abundance than Li or B and had a lower sensitivity factor making its detection difficult in these samples.

METHODS

Presolar SiC grains were obtained from two sources. Ten SiC grains isolated from the Murchison meteorite by our new "gentle separation" (GS) procedure were analyzed along with eleven SiC grains separated by the acid residue (AR) process (Amari et al. 1994) (KJG, nominal size range 1.5–3 μm). Two GS grain samples were created from the 1.4 μm to 17 μm size separation (C4) and the 0.4 μm to 1.4 μm size separation (D4) (Tizard et al. 2005). The grains from these two samples were held in suspension in a few microliters of pure water with isopropanol and distributed thinly over the high-purity gold foils imprinted with copper finder grids for reference of grain locations. SiC grains were located on the GS sample by mapping of large areas in C, O, Mg, Fe, and Si with a Cameca SX100 electron probe. SiC grains from both samples were then verified for SiC composition by EDS analysis and imaged at high resolution using a JEOL 6400 SEM and a Phillips XL30 environmental SEM (ESEM). Grains on each sample were given a nomenclature in the sequence of: separation procedure (AR or GS), sample designation (1 or 2 for the AR samples and C4 or D4 for the GS samples), and location on the imprinted grid (letters A–Z, each subdivided into quadrants numbered 0–3), followed by a numbered sequence of grains within the area of that letter/quadrant.

A time-of-flight secondary ion mass spectrometer (TOFSIMS) instrument based on the BIOTOF design (Braun et al. 1998) was used to acquire high spatial resolution and high mass resolution analyses and is described in detail elsewhere (Henkel et al. 2006, Forthcoming). A 25keV Ga+ primary ion beam was rastered over the sample to sputter secondary ions, which were then mass analyzed by time-of-flight mass spectrometry. A significant advantage of TOFSIMS is that all elements are detected simultaneously. The low duty cycle of the pulsed ion beam of TOFSIMS means that the sputtering rate of grains is very much slower than SIMS using a DC ion beam and surface coatings may be studied. Rastering the primary ion beam across the sample builds up an image of the sample with each pixel containing a complete mass spectrum. The grains were analyzed using a Ga primary ion beam with spot size focused to ≈300 nm and chopped into pulses between approximately a few ns to 20 ns. These gave mass resolutions ranging from ≈2300 (defined as full width at half maximum height) for analysis of the Si isotope ratios of the grains to ≈300 for analysis of Li and B abundances and isotope ratios. Mass interferences at masses 6–11 are minimal and were assessed by analyzing a range of minerals with minimal Li or B but covering the range of major and minor elements found in SiC grains. Background counts from mass interferences were assessed as contributing less than 2% of the count rate for Li and B and was within the counting statistics error of the measurements. Longer pulse lengths of 10–20 ns (which gave lower mass resolution ≈300) were used to increase the average primary current hitting the sample, and thus increasing signal collection rates.

The primary ion beam was rastered over the field of view (tailored to individual grain size) to build up an image. A complete mass spectrum (1–600 amu) was accumulated for each pixel in the image of the raster area. The spatial resolution of ≈300 nm provided clear grain boundaries and some detail of heterogeneous areas within grains. Data were selected from the grain area only, to ensure no background signal contributed to the spectrum. Blank surfaces of gold foil were also measured in several places on each sample to check for sample contamination. No significant signal was found, indicating that there was no contamination during sample preparation and handling.

When determining silicon isotope ratios, the most significant interference was ^{28}SiH on ^{29}Si. ^{28}SiH/^{29}Si was usually in the range 1 to 3 with the contribution of the low mass tail of ^{28}SiH at ^{29}Si being up to 0.3 of the ^{29}Si peak height. The mass resolution of ≈2300 at ^{29}Si enabled hydride interferences to be deconvoluted (using algorithms described by Stephan [2001]) when determining element abundances and isotope ratios. The deconvolution was shown to be accurate by analysis of terrestrial standards although the presence of the ^{28}SiH interference typically added 20–30‰ uncertainty in the derived δ^{29}Si value.

Depth Profiling

Sputtering is a destructive process that removes atoms up to a depth of a few nm from the surface. Prolonged sputtering removes successive sections through the grain, enabling the construction of a three-dimensional profile. Hydrocarbons

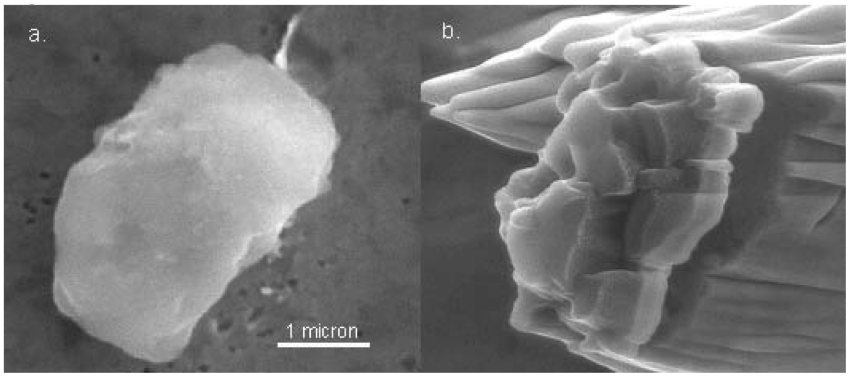

Fig. 1. SEM and environmental SEM images of gently separated presolar SiC GS-D4-G2-1. a) Before and (b) after TOFSIMS analysis. a) The original grain before sputtering and (b) the sputtered SiC grain is sitting on a pedestal of gold that has been eroded around it. The primary Ga+ beam was incident on the grain from the left side of the image.

from the ultra-high vacuum environment tend to deposit on the surface over time, so some cleaning of the surface was also required prior to analysis. The procedure followed was therefore to raster the primary ion beam for ~30 s over a 100–200 μm area that included the grain, which removed ~1 nm of material, cleaning the grain surfaces. Zooming in the DC beam to a smaller rastered area (~10 μm) centered on the grain removed more material, depth profiling into the grain. Cleaning and depth profiling procedures were interleaved with secondary ion data acquisition formed by pulsed ion beam measurements. Since the primary ion beam only sputters the grain for a few ns at a frequency of a few kHz, the sputtering rate during analysis is very much slower than during the use of a DC beam. However, since data acquisition can continue for up to several hours, sputtering can be significant over this length of time. Calculating the effective depths from which the analyses were obtained therefore required careful accounting of the sputtering of the grain surface through these different procedures. Estimated sputter depths for each individual measurement are given in the Appendix.

At the start of the analysis, secondary ions are sputtered from the outer coating of the grain. After some time, that surface is removed and the core exposed. But even an idealized depth profile will not record the true elemental abundances of the core, as there will still be some contribution from the remaining coat surrounding the grain. If there is a strong elemental gradient, as here, then this significantly affects the measured core elemental abundances. A further complicating geometrical effect for a three-dimensional body is varying angle of incidence between the primary ion beam and different points on the surface, which results in different sputtering rates between the part of the grain for which the ions impact normally and those areas of the grain that are sputtered by ions at a lower angle to the surface normal. The spatial resolution of the Ga+ beam of ~300 nm therefore means that the Li/Si and B/Si ratios given here for the cores of the grains are likely to be upper limits. SEM images of one of the gently separated grains is shown in Fig. 1 (before and after TOFSIMS analysis).

Elemental abundance and isotopic data were calibrated by thorough quantification of terrestrial standards. Relative sensitivity factors (RSF) were derived from seven MPI-DING silicate standards (Jochum et al. 2000) and two NIST standard reference materials SRM611 and SRM112b (Henkel et al. 2006). Measured elemental abundances are known to vary when analyzed in samples of different mineralogy due to matrix effects (McPhail 2006). It is therefore important to calculate RSFs from a material similar to that intended for analysis. One terrestrial SiC standard (SRM112b) was measured for comparison to the quantified RSFs of the silicate standards. However, because only a few elements are quantified for this standard it is not suitable for the overall calibration. Measurements of the elemental abundances in the terrestrial SiC standard showed an elevation of a factor of 3 on average in all quantified minor element abundances compared to the silicate standards. It is our conclusion that a consistent variation of all elements relative to Si indicates a reduction of factor of 3 in the Si yield of the SiC matrix compared to the silicate standards. We therefore corrected for this change in Si yield in all SiC samples measured. Isotopic mass fractionations from the sputtering process for Si, Li, and B were derived from an average of multiple analyses from the NIST and MPI-DING standards (Henkel et al., Forthcoming). Isotopic data presented here have been corrected for this fractionation.

Lithium has a much higher ionization probability (relative sensitivity factor) for positive ions during secondary ionization than boron (ionization efficiencies of 24.8 and 1.58, respectively, relative to silicon in silicates) (Henkel et al. 2006). This means that lithium abundances and isotope ratios were much easier to analyze to lower detection levels than was possible for boron.

Six silicate (olivine and pyroxene) grains isolated from the meteorite matrix by the gentle separation technique were also analyzed to assess whether contamination during the extraction process could affect the measured Li and B element abundances.

Table 1. Measured silicon isotope ratios, δ^{26}Mg values, and ^{7}Li/^{6}Li and ^{11}B/^{10}B ratios for acid residue grains and gentle separation grains analyzed as part of this study.[a]

	Grain size (μm)	δ^{29}Si	δ^{30}Si	δ^{26}Mg	^{7}Li/^{6}Li	^{11}B/^{10}B
AR grains						
AR1-M2-1	2 × 1.4	60 ± 40	90 ± 40	90 ± 220	11.5 ± 1.2	4.0 ± 0.4
AR1-M2-2	0.9	20 ± 50	11 ± 17	220 ± 160	13.3 ± 4.3	n.d.
AR1-M2-3	0.8	10 ± 120	30 ± 90	n.d.	11.0 ± 2.1	n.d.
AR1-R-1	2	50 ± 120	–20 ± 50	–370 ± 260	13.4 ± 2.5	3.6 ± 0.3
AR2-S0-1	1.9	n.d.	160 ± 70	–20 ± 60	13.3 ± 1.2	n.d.
AR2-S0-2	1.2	130 ± 70	140 ± 60	–70 ± 40	11.6 ± 1.0	3.0 ± 0.8
AR2-S0-3	1.3	240 ± 100	60 ± 50	–8 ± 23	12.2 ± 0.5	3.2 ± 0.9
AR2-S0-4	2	n.d.	120 ± 80	120 ± 50	11.9 ± 1.0	5.0 ± 2.4
AR2-S3-1	~2.1	n.d.	50 ± 60	–100 ± 140	12.7 ± 1.0	n.d.
AR2-S3-3	~1.4	70 ± 80	40 ± 70	–80 ± 70	12.3 ± 0.7	2.7 ± 0.6
AR2-30-1	4 × 1.4	n.d.	200 ± 60	n.d.	15.8 ± 2.1	n.d.
GS grains						
C4-K2-1	~2	100 ± 60	122 ± 17	0 ± 4	12.0 ± 0.4	3.7 ± 0.4
C4-K2-2	~2.6	0 ± 100	100 ± 40	28 ± 12	11.1 ± 0.6	3.4 ± 0.8
C4-R-1	5 × 6.5	20 ± 90	9 ± 26	–22 ± 8	14.5 ± 2.5	4.8 ± 0.9
D4-Y1-2	5.1 × 3.5	40 ± 110	60 ± 80	90 ± 30	9.9 ± 2.5	1.3 ± 1.0
D4-E-1	~1	70 ± 180	40 ± 140	10 ± 50	10.6 ± 1.9	2.2 ± 1.3
D4-G2-1	4.9 × 2.7	190 ± 210	150 ± 70	–50 ± 60	13.7 ± 0.9	3.8 ± 0.9
D4-K1-1	3.3 × 2.6	40 ± 110	60 ± 50	–10 ± 40	11.7 ± 0.6	3.6 ± 0.3
D4-K1-2	~1	n.d.	n.d.	n.d.	7.2 ± 2.6	3.0 ± 3.5
D4-Y1-1	~1	230 ± 230	30 ± 60	360 ± 50	10.4 ± 0.8	4.4 ± 0.8
D4-Y1-3	2.4 × 2	200 ± 100	50 ± 60	20 ± 80	10.8 ± 0.7	4.0 ± 0.7

[a]Errors are 1σ; n.d. = not determined.

RESULTS

The δ^{29}Si and δ^{30}Si measured values of the grains (both acid residue and gently separated grains) are all within the range –20‰ to +240‰ (Table 1; Fig. 2). These measurements categorize them as probably being mainstream grains (Bernatowicz and Zinner 1997), condensed in the envelopes of 1–3M_{solar} AGB stars of solar metallicity. Only one grain, GS-D4-Y1-1, showed a significant but small ^{26}Mg-excess from the decay of ^{26}Al resulting in an inferred initial ^{26}Al/^{27}Al ratio of 2.9(±1.0) × 10^{-3}. No other grains exhibited δ^{26}Mg values that were significantly above 0‰. X grains have ^{26}Al/^{27}Al ratios in the range 0.02 to 0.6 whereas mainstream grains have ^{26}Al/^{27}Al in the range 10^{-4} to 10^{-3} (Hoppe and Ott 1997). This reinforces the conclusion that none of the grains analyzed were X grains. Within the error bars, the grains cannot be distinguished between mainstream and A, B, Y, or Z grains (Hoppe and Ott 1997). However, given the high relative abundance of mainstream grains (>90%), they are likely to be mainstream although there is a 26% probability that 2 of the analyzed grains may be of type A, B, Y, or Z.

The Li and B isotopic ratios, averaged for each grain, are all within 2 standard deviations of solar system average values and clearly distinguished from production by spallation which has ^{7}Li/^{6}Li ≈ ^{11}B/^{10}B ≈ 2.5 (Casse et al. 1995; Meneguzzi et al. 1971).

Very high Li/Si and B/Si abundances were found which varied by up to 3 orders of magnitude. A good correlation was found between B/Si and Li/Si abundance ratios, as shown in Fig. 3 from analyses of both AR and GS grains. Furthermore, successive analyses when sputtering into the grain, which exposed more of the core of the grain, showed systematically lower abundance ratios of B/Si and Li/Si down towards a value of ~10^{-5}. These measured values are shown in Fig. 3 along with a dotted line representing an equal atomic abundance ratio of Li/B = 1. If, initially, the measurements were off the dotted line in Fig. 3 then the acquired Li/Si and B/Si ratios first tended to move towards the dotted guide line with successive measurements and then down towards solar abundance values.

An obvious possible interpretation of the Li-B correlation is that the SiC grain surfaces were contaminated by Li and B of solar system isotopic composition, either in the presolar nebula, or within the meteorite (perhaps during early aqueous alteration), or during the extraction procedure (either acid residue or gentle separation). To test these possibilities,

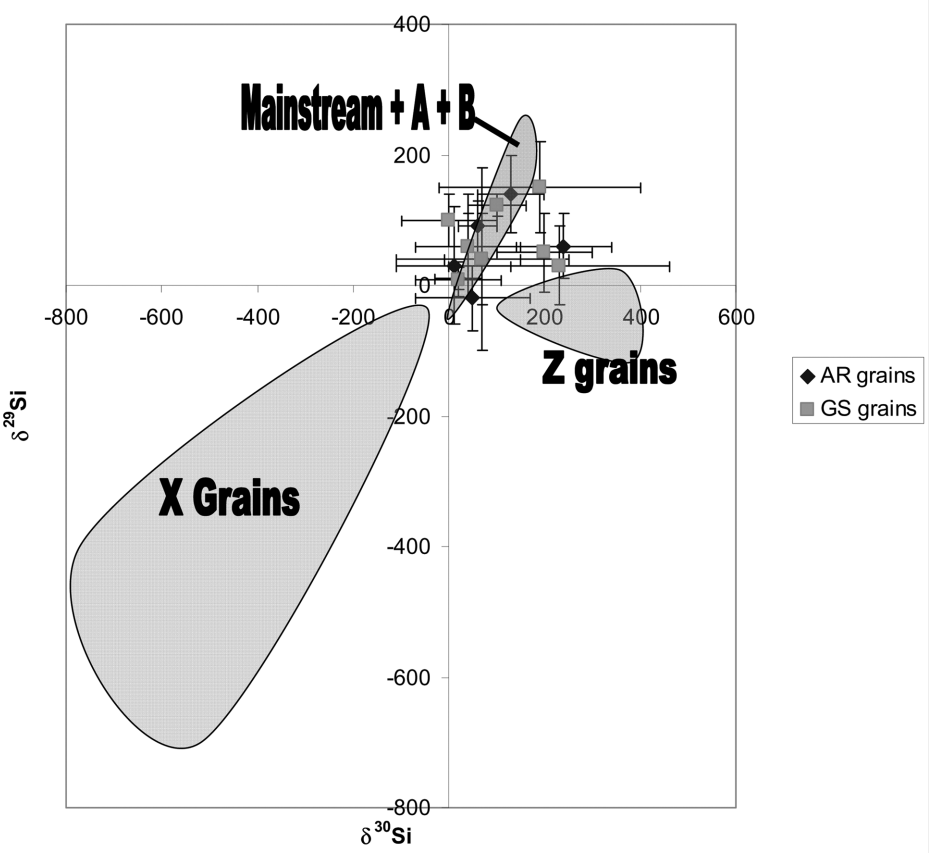

Fig. 2. Analyzed Si isotope ratios of SiC grains reported in this study. Also shown are approximate fields that define different grain types (modeled after Hoppe and Ott [1997]). Here $\delta^{n}Si = 1000 \times [(^{n}Si/^{28}Si)_{sample}/(^{n}Si/^{28}Si)_{standard} - 1]$.

6 silicate matrix grains were also analyzed from the same size and density separate that produced the gently separated SiC grains. No boron was detected in the grains (upper limit on B/Si ~10^{-5}) and, although lithium was just detected as a background signal, Li/Si < 10^{-5} was found.

TOF-SIMS imaging showed the B and Li to be strongly localized to the grains with almost no measurable background from the gold foil on which the grains were deposited. To illustrate this, Fig. 4 shows ^{28}Si, ^{7}Li, ^{11}B, and ^{12}C positive ion images for grain GS-C4-K2-1. The ionization efficiency for B is much lower than for Li and that of C very much lower than Si, making the number of counts for B and C much lower than for Li and Si, respectively. Nevertheless, a background that is essentially zero outside these mass peaks means that even small signal counts can be unambiguously identified.

An additional argument against surface contamination is the observation that although Li and B were concentrated at the surfaces of the acid residue grains, the maximum Li/Si and B/Si ratios were often found below the surface in the gently separated grains (Fig. 5). The high Li and B abundances were not leached by the acid treatment in AR grains implying that they may not have been surficial but present at a small depth within the surface.

DISCUSSION

Preferential sputtering and ionization of some elements at sample surfaces is known, particularly if there is a surface oxide layer. We first address whether such effects could cause the observed large decreases in Li/Si and B/Si ratios during depth profiling.

We were not able to obtain depth profiles for Li/Si and B/Si on the matrix grains for comparison with SiC grains as Li and B were at too low levels to be detected in the matrix grains. However, we show in Fig. 6 that depth profiles of Na/Si, K/Si, Mg/Si, Ca/Si, Al/Si, and Fe/Si, where these elements are major constituents of the mineral structure (and therefore relatively uniform throughout the grain), do not show a decrease with depth or only a small decrease with depth in the case of Na and a small drop between the first two data points for K. Some of the Na and K is unlikely to be structural, however, as Na and K are ubiquitous over many surfaces and appear on any sample analyzed by SIMS until sputtered away. At least part of the observed decrease in Na/Si and K/Si with depth is therefore likely to have resulted from surface contamination of Na and K on the grains. The ionization behavior of Li and B in SIMS would be expected to be similar to the above measured elements and thus give no grounds for

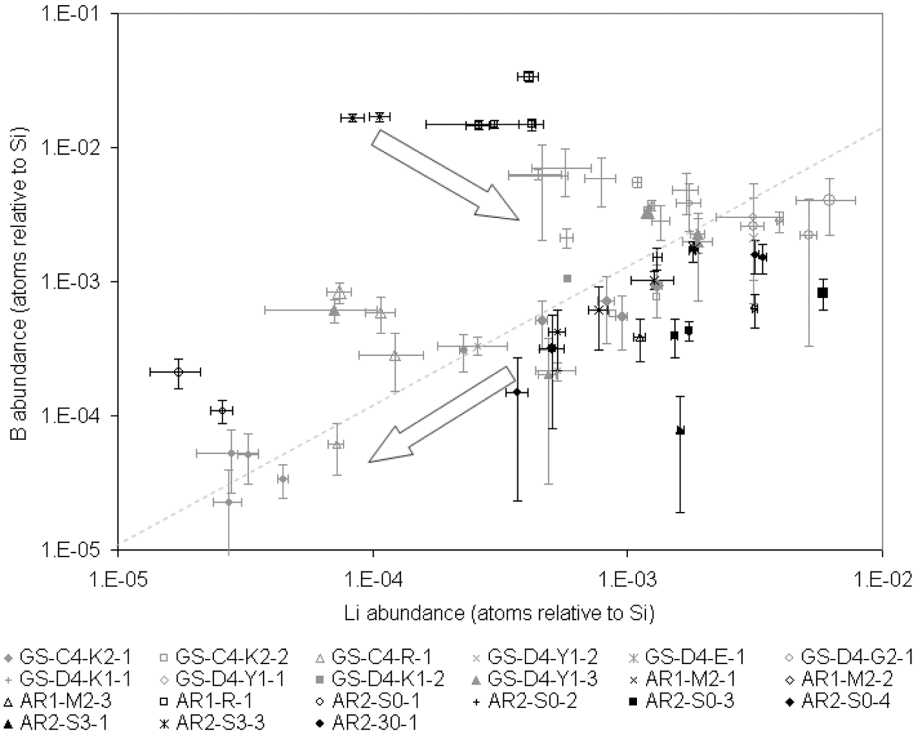

Fig. 3. Measured B/Si and Li/Si abundances in a set of 11 acid residue (AR) and 10 gently separated (GS) grains. Each grain is denoted by a symbol, given in the legend, with 1σ-error bars. GS grains are indicated by gray symbols, AR grains are indicated by black symbols. Decreasing size of the symbols indicates successive measurements taken at depth as the grain surface is sputtered. The dotted line is a line of equal abundance for Li and B. The arrows show how successive measurements acquired on particular grains change as the grain is sputtered.

explaining the measured decrease in Li/Si and B/Si with depth as a sputtering artifact.

An additional argument against the measured profiles being a sputtering artifact is that depth profiling using secondary ionization is a well-established technique, widely used to determine the abundances of many elements in samples. Boron in silicon is regularly measured by researchers in the semiconductor industry. Only minor preferential sputtering effects have been observed (e.g., McPhail 2006).

These results lead us to argue that preferential sputtering or ionization cannot account for more than a small factor (probably no more than a factor of 2) in the decreasing Li/Si and B/Si ratios with depth and that the measured decrease is real and due to a large decrease in abundance of these elements in the cores of the grains.

The low abundance ratios of Li/Si and B/Si in bulk meteorite matrix of ~10^{-5} (Curtis et al. 1980) imply that the measured high Li/Si and B/Si abundance ratios at the surfaces of AR grains cannot have been caused by lithium and boron dissolved from the meteorite matrix during the acid extraction process and deposited on the surfaces of the remaining grains. Similarly, the very low Li and B abundances measured on the surfaces of the 6 random matrix grains argues that there was no contamination of grains after they were deposited on the gold sheet. We therefore argue that the high Li/Si and B/Si abundances that we measured were not caused by contamination from solar system Li and B either by aqueous alteration in the meteorite or during the extraction process (acid residue or gentle separation). Therefore, the measured high B and Li elemental abundances in the surfaces of SiC grains were formed either in an extrasolar environment or in the protosolar nebula during the epoch when the SiC grains were present in the collapsing molecular cloud that went to form the solar system.

Previous studies of Li and B abundances in acid residue mainstream SiC and "X" (supernova) grains (Hoppe et al. 2001; Huss et al. 1997) showed variable abundances of B and Li, but with isotope ratios indistinguishable from solar system average. The abundance ratio of B/Si found in supernova SiC "X" grains (Hoppe et al. 2001) at ~1×10^{-5} was an order of magnitude lower than predicted by condensation models (Hoppe et al. 2001). B/Si abundance ratios were found to range between 1×10^{-5} and 1×10^{-3} in Murchison mainstream SiC grains (Hoppe et al. 2001) and B/Si and Li/Si abundance ratios found to vary between ~1×10^{-6} and 1×10^{-4} in Orgueil SiC grains (Huss et al. 1997). Thus, although the range of values we measured in the near surface of the gently separated grains is higher than measured previously, the abundances in the core of the grains drop to values comparable to what has been measured previously (Hoppe et al. 2001; Huss et al. 1997) and the

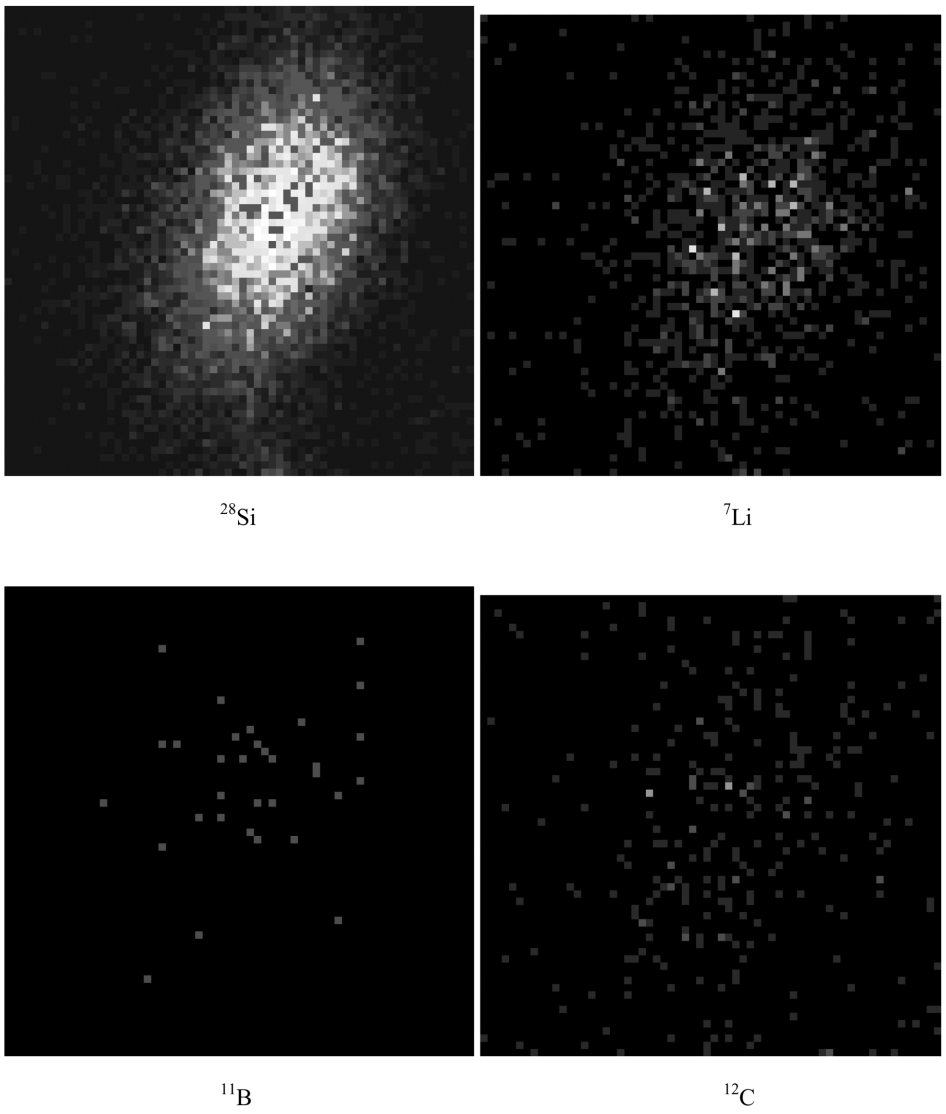

Fig. 4. Ion maps of grain GS-C4-K2-1 in Si, Li, C, and B. Image size is 5 μm.

isotopic compositions are consistent with previous measurements.

Lithium and boron elemental and isotopic abundances play a significant but often overlooked role in understanding galactic chemical evolution (GCE). ^{6}Li, ^{7}Li, ^{10}B, and ^{11}B are easily destroyed in stars and synthesized and destroyed to very different degrees in different astrophysical environments making them (potentially) powerful tracers of processes in those environments.

Models of high-energy cosmic-ray spallation in the interstellar medium (Casse et al. 1995; Meneguzzi et al. 1971) predict an ^{11}B/^{10}B isotope ratio of ≈2.5, and yet with only minor variation, measurements of ^{11}B/^{10}B in solar system materials (Hanon et al. 1999) and presolar grains (Hoppe et al. 2001; Huss et al. 1997) yield an ^{11}B/^{10}B isotope ratio of ≈4. Two supplemental sources for ^{11}B production have been suggested which could raise the ^{11}B/^{10}B ratio from ≈2.5 for high energy cosmic ray spallation to the solar system value of ≈4: i) low energy galactic cosmic ray (GCR) spallation between C and O nuclei and interstellar H and He in star-forming regions (Casse et al. 1995; Ramaty 1996), and ii) type II supernovae (Woosley et al. 1990; Yoshida et al. 2001), which may produce ^{11}B by neutron-induced (ν-process) spallation of C nuclei in the C-rich layers of the star or with alpha captures on lithium in the He layer. These processes are thought to heavily enrich the supernova ejecta in ^{11}B.

^{7}Li is thought to be mainly primordial, synthesized in the Big Bang whereas ^{6}Li is only known to be produced by spallation. Mixing of diverse sources of lithium in the different regions that the grains have experienced could therefore in principle yield ^{7}Li/^{6}Li ratios in solar system materials ranging from ≈2.5 from spallation (Casse et al. 1995; Meneguzzi et al.

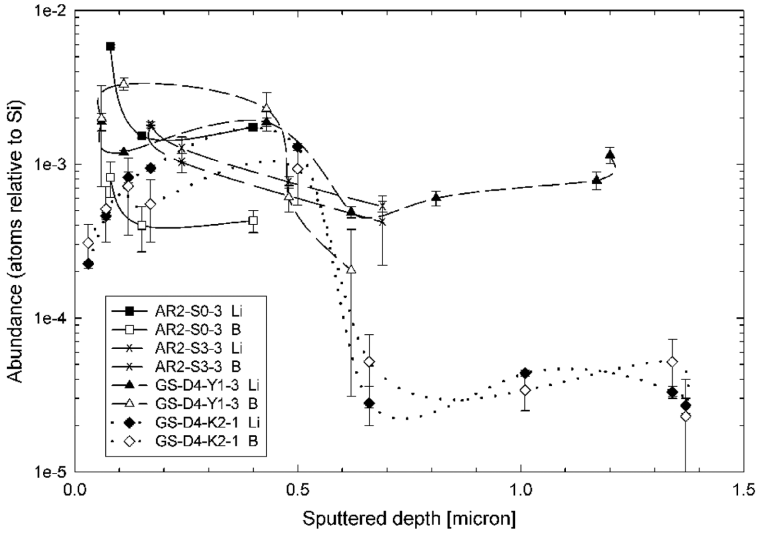

Fig. 5. Li/Si and B/Si abundance ratios with estimated sputtered depth in grains AR2-S0-3, AR2-S3-3, GS-D4-Y1-3, and GS-C4-K2-1. GS grains show an initial rise in their Li and B abundances with sputter depth before a steep decrease toward solar abundance, whereas AR grains show a direct decrease from the top surface. Error bars are 1σ.

1971) to enormously high values for Li formed in the Big Bang. However, the average solar system $^{7}Li/^{6}Li$ ratio is ≈12 and, like boron, lithium displays almost monotonous isotopic uniformity across a range of extraterrestrial materials. (Two exceptions are a ±40‰ systematic variation $^{7}Li/^{6}Li$ in chondrules from the Semarkona meteorite ascribed to incomplete mixing of different Li sources in the early solar system (Chaussidon and Robert 1998) and a measurement of $^{7}Li/^{6}Li \approx 30$ in implanted solar wind (Chaussidon and Robert 1999). The latter value, however, is ascribed to preferential destruction of ^{6}Li in the Sun).

Spectroscopic measurements of interstellar clouds in the direction of *o* Per (Knauth et al. 2003) revealed a $^{7}Li/^{6}Li$ ratio of ~2 but in other directions, star-forming regions have a value of $^{7}Li/^{6}Li \approx 12$ very close to the solar system (Knauth et al. 2003). These authors conclude that most of the material in the solar neighborhood has approximately solar-system Li isotope ratios. A spectroscopic measurement of $^{11}B/^{10}B = 3.4$ (+1.3–0.9) was also obtained for the Orion molecular cloud (Federman et al. 1996).

The measured depth profiles for Li/Si and B/Si in the grains showing a lower surface abundance ratio rising to a peak within the grain then falling to low levels implies an implantation mechanism. In the GS grains, the abundance distribution peaks at a depth of ~0.2–0.4 μm. Experimental measurements and theoretical modeling of implantation depths of light atomic species into SiC (Chakarov and Temkin 2005; Lee and Park 2002; Verchovsky et al. 2001; Verchovsky et al. 2004) imply a kinetic energy of Li and B ions relative to the grains of ~100–200 keV. This corresponds to a velocity of up to 1200–1800 km s^{-1} for these ions. Measurements of abundance and isotopic composition of noble gases in presolar SiC as a function of grain size support this model since they too strongly suggest implantation of noble gas ions into grains with these typical energies (Verchovsky et al. 2001; Verchovsky et al. 2004).

Cosmic rays can be ruled out as a source of the Li and B despite the known high abundance of Li, Be, and B in cosmic rays and the ISM produced by the inverse spallation process (LiBeB/CNO ~ 0.25) (Vangioni-Flam et al. 2000) on the grounds of the isotopic composition $^{7}Li/^{6}Li \approx {}^{11}B/^{10}B \approx 2.5$, in cosmic rays. In situ spallation can also be ruled out as a source, since cosmic ray energies peak at 100 MeV and atoms of this energy have ranges of tens of microns in SiC which is far larger than the grains. Although there may be some Li and B in situ production by spallation within the grain caused by cosmic rays, the spallation products would have a homogenous distribution within the grains which is not what is found. In situ production of Li and B by cosmic ray spallation in the grain can therefore at most account for a small percentage of the observed Li and B abundances within the grains.

Our data are thus most consistent with an implantation of Li and B of approximately solar system isotopic composition and velocities of ~1200–1800 km s^{-1} into the SiC grains.

To try and hypothesize where the grains may have acquired the high Li and B abundances with solar-like isotope ratios, we bear in mind that there are 5 main regions that the grains likely experienced: 1) the AGB star that formed the grain, 2) the diffuse interstellar medium (in the sense of less dense regions between older stars), 3) denser star-forming regions that the grain may have passed through, 4) the star-forming region that the Sun was in as it formed, and 5) the protosolar nebula. The grain may have passed through star-forming regions and the diffuse interstellar medium multiple times.

For reasons outlined earlier we have already discounted alteration within the meteorite or contamination during grain extraction as sources of the high Li and B abundances. Similarly the bulk material of the protosolar nebula is only likely to have had low Li/Si and B/Si ratios on average (since Li/Si and B/Si ratios in the Sun are ~10^{-5} [Anders and Grevesse 1989]) and so we do not see that as a viable source for the very high Li and B abundances. Models of the early solar nebula that invoke an "X" wind producing the high Li and B abundances either by implantation or in situ in the grain would have great difficulty in producing the solar-like isotope ratios reported here (Gounelle et al. 2001).

There are Li-rich AGB stars which may have been able to supply the very high Li abundances seen here through the Cameron-Fowler mechanism in which α particles react with ^{3}He nuclei to produce ^{7}Be which decays to ^{7}Li (Sackmann and Boothroyd 1999). However, this process does not produce ^{6}Li so implantation of ^{7}Li into the grain directly from the star would not give the solar ^{7}Li/^{6}Li isotope ratio. K giants do however release circumstellar shells with high ^{7}Li, seeding the surrounding region (De la Reza 2000). Some of these regions are observed to have very high Li, B abundances and solar-like Li and B isotope ratios by mixing high abundances of spallation Li and B with high ^{7}Li and ^{11}B abundances (Chaussidon and Robert 1999; Hobbs 2000; Yoshida et al. 2001). The giant star that produced the high Li abundances need not necessarily have been the same star that formed the SiC grains but only that it seeded the region through which the grains were traveling.

It seems likely to us that the uniformity of Li and B isotopic compositions measured within so many different regions—the solar system (Chaussidon and Robert 1998; Chaussidon et al. 1998; Hanon et al. 1999; Robert and Chaussidon 2003), spectroscopically in many star-forming regions (Federman et al. 1996; Knauth et al. 2003), and in presolar grains (Hoppe et al. 2001), and in the present work—results from mixing of very different sources on a molecular cloud scale.

Germane to our discussion here is the model of Verchovsky et al. (2004) who found a dependence of noble gas concentration and isotopic composition with grain size in presolar SiC grains. Smaller grains were, relative to their size, much more gas rich (in noble gas concentration, cm^3 g^{-1}) than larger grains. Furthermore, there was a change of isotopic composition in, for example, the Kr-s component which they explained as resulting from two noble gas sources with different energies which were therefore implanted to different depths in the grains. The two isotopically different components with different energies resulted from i) the low-energy component from the stellar wind from the main stage of the evolution of AGB stars, and ii) the high-energy component from the late-stage, post-AGB planetary nebula phase. They further explained measured differences between the abundances of different noble gases in the grains as resulting from differences in ionization potential for the different elements. He, Ne, and Ar have higher ionization potentials than Kr and Xe, so that the latter were more likely to be ionized and accelerated by magnetic fields in the environment of the AGB star or in the planetary nebula phase. The inferred velocities of the implanted noble gas atoms in the high energy planetary nebula phase were ~1500 km s^{-1}.

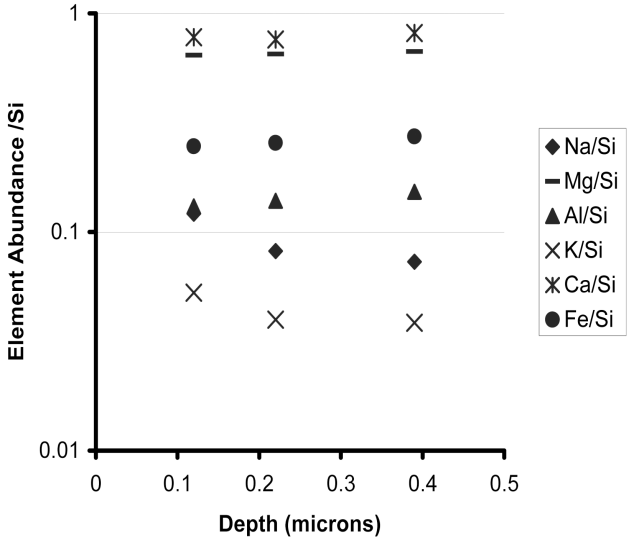

Fig. 6. Measured Na/Si, K/Si, Mg/Si, Ca/Si, Al/Si, and Fe/Si ratios as a function of depth in a non-SiC grain with these elements as major components.

In the work presented here, we have inferred a relative velocity of ~1200–1800 km s^{-1} between the grain and implanted atoms. There is therefore good agreement on this point between our data and the model of Verchovsky et al. (2004) if the Li and B atoms were implanted by the same mechanism of high energy ions accelerated in the planetary nebula phase of the AGB star that formed the SiC grain. The ionization potentials of Li and B are respectively 5.39 eV and 9.32 eV which are both lower than the ionization potentials of Xe and Kr (12.13 eV and 14.00 eV, respectively). Thus if Xe are Kr are ionized, accelerated, and implanted in the Verchovsky et al. model, so too will be Li and B. This model therefore seems plausible for explaining the data presented in this paper except for one factor, that of the isotopic composition of Li and B which are the same as average solar system material. It seems to us unlikely that Li and B implanted in the SiC grains directly from an AGB star would have exactly this isotopic composition. Above we have argued that the uniformity of measured Li and B isotope ratios represent mixing between many sources. Thus, the Verchovsky et al. model is attractive but on these grounds we think it unlikely to explain the present data, although we do not rule it out.

If the argument is accepted that the ^{7}Li/^{6}Li ≈ 12, ^{11}B/^{10}B ≈ 4 isotopic composition can only be achieved by mixing of many sources, it follows that the Li and B we have measured in the SiC grains must have been implanted into the SiC grains after being mixed from many sources. The

environment that this could happen would have to have been a molecular cloud or region of density higher than typical interstellar medium with Li and B isotopic composition ($^7Li/^6Li \approx 12$, $^{11}B/^{10}B \approx 4$) similar to those measured spectroscopically (Federman et al. 1996; Knauth et al. 2003). Knauth at al. (2003) conclude that almost all the material in the solar neighborhood has $^7Li/^6Li \approx 12$. Shocks in the molecular cloud, such as from supernovae could be the mechanism by which the atoms were accelerated and implanted into the grains. There is no evidence that the grains themselves were formed by supernovae as they are not "X" grains but shock waves from a supernova do exceed 5×10^3–10^4 km s^{-1} (Ellison et al. 1997; Reynolds and Ellison 1992) and when they interact with molecular clouds, can compress the material, accelerating it. Other shock mechanisms such as the planetary nebula stage of AGB stars discussed by Verchovsky et al. (2004) may also provide the accelerating mechanism for atoms and ions within the molecular cloud. Such models seem plausible but detailed modeling is beyond the scope of the present paper.

CONCLUSION

We have measured highly elevated Li/Si and B/Si abundance ratios in the outer parts of presolar SiC grains compared with the cores of the SiC grains. The $^7Li/^6Li$ and $^{11}B/^{10}B$ isotope ratios of the grains are the same as for average solar system matter within the confidence limits of the measurements. Depth profiling of the Li/Si and B/Si abundance ratios in the grains shows a maximum value below the surface which we interpret as implantation by energetic Li and B ions or atoms into the grains. In trying to understand the source of energetic Li and B ions or atoms, we rule out the diffuse interstellar medium since the energies of atoms and isotopic composition of Li and B from the interstellar medium are incompatible with the measurements. We have ruled out implantation of Li and B into the grains in the protosolar nebula on the grounds that the Li and B abundances in the nebula are probably too low. We have also ruled out alteration of grains in the early solar system or during the laboratory extraction process since the abundance profile with depth in the grain is most consistent with an implantation profile and not surface contamination.

Our interpretation of the abundance depth profile of Li and B in the grains as due to implantation implies Li and B ions impacting the grains with velocities in the range of 1200–1800 km s^{-1}.

Our model for the depth profile pattern and isotopic composition of Li and B in these SiC grains therefore is that the SiC grains were condensed in the outflow of an AGB star and later acquired high Li and B abundances in their outer layers by implantation from fast-moving shock fronts in a denser molecular cloud region. The isotopic compositions of the implanted Li and B in the grains are within error identical to the isotopic composition of solar system material and also spectroscopic measurements of Li and B in denser nearby star-forming regions. We interpret this uniformity as mixing of diverse sources of Li and B into denser molecular clouds and shock waves implanting this homogenized Li and B into SiC grains passing through the clouds.

The study of other elements that may also have been implanted into presolar SiC grains will prove interesting and informative for this model.

Acknowledgments–We thank G. Turner, J. Gilmour, and M. Grady for extremely helpful discussions; D. Blagburn and B. Clementson for technical assistance; S. Amari and R. Lewis for provision of Murchison KJG grains and permission to publish the data; and K. Jochum for provision of MPI-DING standards. We are grateful to P. Hoppe, an anonymous reviewer, and the associate editor, I. Franchi, for constructive reviews which greatly improved the manuscript. We gratefully acknowledge support from the PPARC for funding this work including student work of J. T. and the post of T. H.

Editorial Handling—Dr. Ian Franchi

REFERENCES

Amari S., Lewis R. S., and Anders E. 1994. Interstellar grains in meteorites: I. Isolation of SiC, graphite, and diamond: Size distributions of SiC and graphite. *Geochimica et Cosmochimica Acta* 58:459–470.

Anders E. and Grevesse N. 1989. Abundances of the elements: Meteoritic and solar. *Geochimica et Cosmochimica Acta* 53:197–214.

Bernatowicz T. J. and Zinner E. K. 1997. Astrophysical implications of the laboratory study of presolar materials. In *Astrophysical implications of the laboratory study of presolar materials,* edited by Bernatowicz T. J. and Zinner E. K. Woodbury, New York: American Institute of Physics.

Bernatowicz T., Fraundorf G., Tang M., Anders E., Wopenka B., Zinner E., and Fraundorf P. 1987. Evidence for interstellar SiC in the Murray carbonaceous meteorite. *Nature* 330:728–730.

Bernatowicz T., Messenger S., Pravdivtseva O., Swan P., and Walker R. M. 2003. Pristine presolar silicon carbide. *Geochimica et Cosmochimica Acta* 67:4679–4691.

Braun R. M., Blenkinsopp P., Mullock S. J., Corlett C., Willey K. F., Vickerman J. C., and Winograd N. 1998. Performance characteristics of a chemical imaging time-of-flight mass spectrometer. *Rapid Communications in Mass Spectrometry* 12: 1246–1252.

Casse M., Lehoucq R., and Vangioni-Flam E. 1995. Production and evolution of light elements in star-forming regions. *Nature* 373: 318–319.

Chakarov I. and Temkin M. 2005. Modelling of ion implantation in SiC crystals. *Nuclear Instruments & Methods in Physics Research Section B—Beam Interactions with Materials and Atoms* 242:690–692.

Chaussidon M. and Robert F. 1998. Li-7/Li-6 and B-11/B-10 variations in chondrules from the Semarkona unequilibrated chondrite. *Earth and Planetary Science Letters* 164:577–589.

Chaussidon M. and Robert F. 1999. Lithium nucleosynthesis in the Sun inferred from the solar wind Li-7/Li-6 ratio. *Nature* 402: 270–273.

Chaussidon M., Robert F., Mangin D., Hanon P., and Rose E. 1998. Microscale boron isotope analysis in meteoritic matter. Proceedings, Eleventh International Conference on Secondary Ion Mass Spectrometry. pp. 43–46.

Clayton D. D. and Nittler L. R. 2004. Astrophysics with presolar stardust. *Annual Review of Astronomy and Astrophysics* 42:39–79.

Curtis D., Gladney E., and Jurney E. 1980. A revision of the meteorite-based cosmic abundance of boron. *Geochimica et Cosmochimica Acta* 44:1945–1953.

De la Reza R. 2000. Lithium in giant stars. In *Light elements and their evolution,* edited by Da Silva L., Spite M., and De Medeiros J. R. Dordrecht: Kluwer Academic Publishers. pp. 310–319.

Ellison D. C., Drury L. O'C., and Meyer J.-P. 1997. Galactic cosmic rays from supernova remnants. II Shock acceleration of gas and dust. *The Astrophysical Journal* 487:197–217.

Federman S. R., Lambert D. L., Cardelli J. A., and Sheffer Y. 1996. The boron isotope ratio in the interstellar medium. *Nature* 381: 764–766.

Gounelle M., Shu F. H., Shang H., Glassgold A. E., Rehm K. E., and Lee T. 2001. Extinct radioactivities and protosolar cosmic rays: Self-shielding and light elements. *The Astrophysical Journal* 548:1051–1070.

Hanon P., Chaussidon M., and Robert F. 1999. Distribution of lithium, beryllium, and boron in meteoritic chondrules. *Meteoritics & Planetary Science* 34:247–258.

Henkel T., Stephan T., Jessberger E. K., Hoppe P., Strebel R., Amari S., Zinner E. K., and Lewis R. S. 2002. TOF-SIMS analysis of 13 presolar silicon carbide grains (abstract). *Meteoritics & Planetary Science* 37:A61.

Henkel T., Tizard J., Blagburn D., and Lyon I. 2006. Interstellar dust laser explorer (IDLE): A new instrument for submicron analyses of stardust—Quantification of laser SNMS. *Applied Surface Science* 252:7117–7119.

Henkel T., Tizard J., Blagburn D., and Lyon I. Forthcoming. IDLE—Interstellar dust laser explorer. A new instrument for elemental and isotopic analysis and imaging of interstellar and interplanetary dust. *Review of Scientific Instruments.*

Hobbs L. M. 2000. Lithium. *Physics Reports* 333:449–469.

Hoppe P. and Ott U. 1997. Mainstream silicon carbide grains from meteorites. In *Astrophysical implications of the laboratory study of presolar materials,* edited by Bernatowicz T. J. and Zinner E. K. Woodbury, New York: American Institute of Physics. pp. 27–58.

Hoppe P., Strebel R., Eberhardt P., Amari S., and Lewis R. S. 1996. Small SiC grains and a nitride grain of circumstellar origin from the Murchison meteorite: Implications for stellar evolution and nucleosynthesis. *Geochimica et Cosmochimica Acta* 60:883–907.

Hoppe P., Lodders K., Strebel R., Amari S., and Lewis R. S. 2001. Boron in presolar silicon carbide grains from supernovae. *The Astrophysical Journal* 551:478–485.

Huss G. R., Hutcheon I. D., and Wasserburg G. J. 1997. Isotopic systematics of presolar silicon carbide from the Orgueil (CI) chondrite: Implications for solar system formation and stellar nucleosynthesis. *Geochimica et Cosmochimica Acta* 61:5117–5148.

Jochum K. P., Dingwell D. B., Rocholl A., Stoll B., Hofmann A. W., Becker S., Besmehn A., Bessette D., Dietze H.-J., Dulski P., Erzinger J., Hellebrand E., Hoppe P., Horn I., Janssens K., Jenner G. A., Klein M., McDonough W. F., Maetz M., Mezger K., Münker C., Nikogosian I. K., Pickhardt C., Raczek I., Rhede D., Seufert H. M., Simakin S. G., Sobolev A. V., Spettel B., Straub S., Vincze L., Wallianos A., Weckwerth G., Weyer S., Wolf D., and Zimmer M. 2000. The preparation and preliminary characterization of eight geological MPI-DING reference glasses for in situ microanalysis. *Geostandards Newsletter* 24: 87–133.

Knauth D. C., Federman S. R., and Lambert D. L. 2003. An ultra-high-resolution survey of the interstellar Li-7/Li-6 isotope ratio in the solar neighborhood. *The Astrophysical Journal* 586:268–285.

Lee S.-S. and Park S.-G. 2002. Empirical depth profile model for ion implantation in ^{4}H-SiC. *Journal of the Korean Physical Society* 41:L591–L593.

Lewis R. S., Tang M., Wacker J. F., Anders E., and Steel E. 1987. Interstellar diamonds in meteorites. *Nature* 326:160–162.

McPhail D. S. 2006. Applications of secondary ion mass spectrometry (SIMS) in material science. *Journal of Material Science* 41:873–903.

Meneguzzi M., Audouze J., and Reeves H. 1971. The production of the elements Li, Be, B by galactic cosmic rays in space and its relation with stellar observations. *Astronomy and Astrophysics* 15:337–359.

Nittler L. R. and Alexander C. M. O'D. 2003. Automated isotopic measurements of micron-sized dust: Application to meteoritic presolar silicon carbide. *Geochimica et Cosmochimica Acta* 67: 4961–4980.

Nittler L. R., Alexander C. M. O'D., Gao X., Walker R. M., and Zinner E. 1997. Stellar sapphires: The properties and origins of presolar Al_2O_3 in meteorites. *The Astrophysical Journal* 483: 475–495.

Ramaty R. 1996. Interstellar gamma-ray lines from low energy cosmic ray interactions. *Astronomy and Astrophysics Supplement Series* 120:C373–C380.

Reynolds S. P. and Ellison D. C. 1992. Electron acceleration in Tycho's and Kepler's supernova remnants: Spectral evidence of Fermi shock acceleration. *The Astrophysical Journal* 399:L75–L78.

Robert F. and Chaussidon M. 2003. Boron and lithium isotopic composition in chondrules from the Mokoia meteorite (abstract #1344). 34th Lunar and Planetary Science Conference. CD-ROM.

Sackmann I. J. and Boothroyd A. I. 1999. Creation of Li-7 and destruction of He-3, Be-9, B-10, and B-11 in low-mass red giants, due to deep circulation. *The Astrophysical Journal* 510:217–231.

Stephan T. 2001. TOF-SIMS in cosmochemistry. *Planetary and Space Science* 49:859–906.

Tizard J., Lyon I., and Henkel T. 2005. The gentle separation of presolar SiC grains from meteorites. *Meteoritics & Planetary Science* 40:335–342.

Tomascak P. B. 2004. Developments in understanding and application of lithium isotopes in the earth and planetary sciences. *Reviews in Mineralogy and Geochemistry* 55:153–195.

Vangioni-Flam E., Casse M., and Audouze J. 2000. Lithium-beryllium-boron: Origin and evolution. *Physics Reports* 333: 365–387.

Verchovsky A. B., Wright I. P., Fiseko A. V., and Pillinger C. T. 2001. A numerical model of ion implantation into presolar grains. *Nuclear Physics A* 688:106C–109C.

Verchovsky A. B., Wright I. P., and Pillinger C. 2004. Astrophysical significance of asymptotic giant branch stellar wind energies recorded in meteoritic SiC grains. *The Astrophysical Journal* 607:611–619.

Woosley S. E., Hartmann D. H., Hoffman R. D., and Haxton W. C. 1990. The n-process. *The Astrophysical Journal* 356:272–301.

Yoshida T., Hashimoto M., and Yamaoka H. 2001. Neutrino nucleosynthesis of Li and B through type II supernova explosions for population II stars. *Nuclear Physics A* 688:436C–438C.

Zinner E. 1998. Stellar nucleosynthesis and the isotopic composition of presolar grains from primitive meteorites. *Annual Review of Earth and Planetary Sciences* 26:147–188.

APPENDIX

Table A1. Individual AR grain data giving average ^{29}Si and ^{30}Si isotope data for each grain, ^{7}Li and ^{11}B isotope data for individual measurements and averages for each grain (in bold), and estimated sputtered depths per measurement and Li and B abundances. Errors are one standard deviation; n.d. = values that couldn't be determined because of too few counts. Values for $^{7}Li/^{6}Li$ and $^{11}B/^{10}B$ ratios in bold at the end of each series of measurements on that grain are the values obtained from the total Li and B counts from all measurements of that grain.

	Grain size	Depth	Isotope ratios				Elemental abundance	
AR grains	(μm)	(μm)	$\delta^{29}Si$	$\delta^{30}Si$	$^{7}Li/^{6}Li$	$^{11}B/^{10}B$	Li/Si (10^{-5})	B/Si (10^{-5})
AR1-M2-1	2 × 1.4	0.12	63 ± 36	94 ± 39	11.4 ± 4.1	3.8 ± 0.5	143.1 ± 5.1	n.d.
		0.31			10.6 ± 3.4	4.2 ± 0.6	62.2 ± 6.5	n.d.
		0.46			12.1 ± 1.5	2.3 ± 4.5	8.4 ± 0.8	1675 ± 121
		0.52			8.9 ± 2.9	n.d.	10.7 ± 1.0	1695 ± 124
					11.5 ± 1.2	**4.0 ± 0.4**		
AR1-M2-2	0.9	0.20	20 ± 41	11 ± 16	19.3 ± 8.4	3.9 ± 4.4	1.7 ± 0.4	21 ± 5
		0.28			12.5 ± 4.5	n.d.	2.6 ± 0.2	11 ± 2
					13.3 ± 4.3			
AR1-M2-3	0.8	0.20	10 ± 118	28 ± 85	11.0 ± 2.1	n.d.	111.6 ± 6.3	39 ± 14
AR1-R-1	2	0.19	50 ± 117	−15 ± 43	15.2 ± 5.6	4.0 ± 0.7	41.0 ± 3.8	3356 ± 260
		0.32			n.d.	4.1 ± 0.9	42.1 ± 4.5	1492 ± 145
		0.48			8.0 ± 2.2	3.9 ± 0.6	29.9 ± 13.8	1498 ± 104
		0.64			14.1 ± 5.7	2.8 ± 0.4	26.0 ± 2.7	1469 ± 110
					13.4 ± 2.5	**3.6 ± 0.3**		
AR2-S0-1	1.9	0.08	n.d.	159 ± 65	13.3 ± 1.2	n.d.	316.6 ± 8.2	63 ± 18
AR2-S0-2	1.2	0.12	130 ± 66	145 ± 55	11.2 ± 1.4	2.8 ± 1.0	179.5 ± 6.0	170 ± 30
		0.17			11.9 ± 1.3	3.3 ± 1.2	130.7 ± 5.0	151 ± 28
					11.6 ± 1.0	**3.0 ± 0.8**		
AR2-S0-3	1.3	0.08	236 ± 97	55 ± 50	12.1 ± 0.8	3.3 ± 1.8	584.9 ± 12.6	82 ± 21
		0.15			11.7 ± 0.6	3.5 ± 1.2	152.8 ± 4.9	40 ± 13
		0.40			14.8 ± 1.8	2.5 ± 1.5	174.3 ± 2.8	43 ± 7
					12.2 ± 0.5	**3.2 ± 0.9**		
AR2-S0-4	2	0.14	n.d.	115 ± 78	12.2 ± 1.6	4.5 ± 3.1	315.1 ± 13.0	159 ± 45
		0.19			11.8 ± 1.3	5.5 ± 3.6	339.5 ± 11.8	151 ± 38
					11.9 ± 1.0	**5.0 ± 2.4**		
AR2-S3-1	~2.1	0.05	n.d.	53 ± 52	12.3 ± 1.5	n.d.	182.4 ± 6.5	n.d.
		0.19			12.9 ± 1.3	3.0 ± 4.2	161.4 ± 4.6	8 ± 6
					12.7 ± 1.0			
AR2-S3-3	~1.4	0.17	65 ± 75	37 ± 68	14.9 ± 1.7	4.4 ± 1.9	182.7 ± 5.6	176 ± 4
		0.24			11.1 ± 0.8	2.0 ± 0.5	126.9 ± 23.7	103 ± 15
		0.48			11.8 ± 3.5	n.d.	76.7 ± 6.5	n.d.
		0.69			10.9 ± 2.9	n.d.	53.1 ± 4.1	42 ± 20
					12.3 ± 0.7	**2.7 ± 0.6**		
AR2-30-1	4 × 1.4	0.08	n.d.	199 ± 60	8.5 ± 3.5	n.d.	87.2 ± 3.6	n.d.
		0.14			22.1 ± 9.4	n.d.	103.0 ± 7.2	n.d.
		0.17			10.7 ± 4.9	n.d.	396.9 ± 33.5	n.d.
		0.24			14.3 ± 7.6	n.d.	66.2 ± 9.1	n.d.
		0.42			11.8 ± 2.9	n.d.	50.7 ± 5.5	32 ± 24
		0.60			14.5 ± 4.3	n.d.	37.1 ± 3.8	15 ± 13
		0.81			12.8 ± 5.2	n.d.	18.3 ± 2.5	n.d.
					15.8 ± 2.1			
Average			79 ± 27	83 ± 19	11.9 ± 0.7	3.6 ± 0.6	131.7 ± 1.8	543 ± 16

Table A2. Individual GS grain data showing the same data as the table for AR grains.

AR grains	Grain size (μm)	Depth (μm)	Isotope ratios				Elemental abundance	
			δ^{29}Si	δ^{30}Si	^{7}Li/^{6}Li	^{11}B/^{10}B	Li/Si (10^{-5})	B/Si (10^{-5})
GS-C4-K2-1	~2	0.03	100 ± 56	122 ± 16	11.6 ± 0.56	3.7 ± 0.5	22.6 ± 0.6	30.8 ± 9.7
		0.07			11.8 ± 1.1	3.3 ± 0.9	46.1 ± 2.5	51.2 ± 20.1
		0.12			11.1 ± 1.4	5.6 ± 3.1	82.3 ± 6.3	72.2 ± 37.5
		0.17			13.7 ± 1.2	3.0 ± 1.0	94.6 ± 4.5	55.1 ± 24.0
		0.50			11.7 ± 1.0	5.5 ± 2.1	130.2 ± 6.5	93.6 ± 39.2
		0.66			8.3 ± 4.8	3.0 ± 2.6	2.8 ± 0.8	5.2 ± 2.6
		1.01			12.8 ± 1.8	4.3 ± 1.8	4.4 ± 0.2	3.4 ± 0.9
		1.34			12.5 ± 2.7	2.8 ± 1.5	3.3 ± 0.3	5.2 ± 2.1
		1.37			19.4 ± 8.8	2.3 ± 1.3	2.7 ± 0.3	2.3 ± 1.7
					12.0 ± 0.4	**3.7 ± 0.4**		
GS-C4-K2-2	~2.6	0.03	5 ± 97	95 ± 33	11.0 ± 0.9	2.8 ± 0.8	87.9 ± 4.1	57.1 ± 23.7
		0.18			11.1 ± 0.9	4.5 ± 1.8	130.1 ± 6.5	76.6 ± 33.8
					11.1 ± 0.6	**3.4 ± 0.8**		
GS-C4-R-1	5 × 6.5	0.03	24 ± 83	9 ± 26	12.7 ± 6.9		12.3 ± 3.5	28.3 ± 13.0
		0.05			21.1 ± 13.8		10.8 ± 1.4	58.9 ± 18.0
		0.07			n.d.	3.6 ± 1.4	7.4 ± 0.8	83.3 ± 15.1
		0.12			13.3 ± 3.7	3.0 ± 2.5	7.2 ± 0.5	6.2 ± 2.6
		0.14			10.0 ± 2.6		8.8 ± 0.7	
					14.5 ± 2.5	**4.8 ± 0.9**		
GS-D4-Y1-2	5.1 × 3.5	0.03	39 ± 103	55 ± 74	4.9 ± 1.8		25.9 ± 7.9	33.3 ± 4.9
		0.09			14.9 ± 5.2	0.6 ± 0.6	53.2 ± 9.4	21.6 ± 3.3
					9.9 ± 2.5	**1.3 ± 1.0**		
GS-D4-E-1	~1	0.12	74 ± 180	36 ± 137	10.6 ± 1.9	2.2 ± 1.3	312.7 ± 35.6	212.7 ± 155.4
GS-D4-G2-1	4.9 × 2.7	0.03	195 ± 209	153 ± 65	11.1 ± 2.2	2.3 ± 1.4	311.2 ± 33.2	261.9 ± 159.8
		0.05			14.0 ± 3.3	6.5 ± 7.6	619.8 ± 159.3	406.8 ± 186.1
		0.21			12.8 ± 1.7	5.9 ± 4.5	512.4 ± 39.3	224.1 ± 190.8
		0.36			15.6 ± 3.1	2.3 ± 1.1	313.6 ± 92.2	303.3 ± 235.4
		0.40			14.2 ± 1.5	3.9 ± 1.5	395.9 ± 12.0	280.8 ± 48.0
					13.7 ± 0.9	**3.8 ± 0.9**		
GS-D4-K1-1	3.3 × 2.6	0.03	43 ± 110	62 ± 49	10.2 ± 2.1	3.8 ± 0.9	44.5 ± 10.6	631.4 ± 55.0
		0.05			12.0 ± 3.0	3.9 ± 0.8	79.0 ± 11.2	593.4 ± 235.3
		0.08			13.2 ± 3.3	3.4 ± 1.0	46.1 ± 12.1	619.7 ± 415.8
		0.14			10.5 ± 4.5	6.7 ± 3.6	57.0 ± 14.7	708.2 ± 275.9
		0.19			11.5 ± 0.7	3.9 ± 0.4	108.9 ± 4.0	550.6 ± 46.3
		0.40			13.8 ± 2.8	7.0 ± 3.4	169.3 ± 19.1	479.5 ± 164.1
		0.73			10.0 ± 2.5	2.6 ± 1.4	135.5 ± 10.8	285.2 ± 81.0
		0.75			13.4 ± 2.9	4.9 ± 1.9	57.9 ± 3.4	212.1 ± 34.2
					11.7 ± 0.6	**3.6 ± 0.3**		
GS-D4-Y1-1	~1	0.24	233 ± 225	32 ± 56	10.1 ± 0.9	4.8 ± 1.0	123.8 ± 3.5	370.2 ± 31.6
		0.30			11.6 ± 2.1	3.1 ± 1.2	175.1 ± 19.5	385.6 ± 147.1
					10.4 ± 0.8	**4.4 ± 0.8**		
GS-D4-K1-2	~1	0.03			7.2 ± 2.6	3.0 ± 3.5	58.4 ± 28.6	104.4 ± 124.3
GS-D4-Y1-3	2.4 × 2	0.06	202 ± 96	50 ± 57	13.1 ± 3.0	2.6 ± 1.6	189.6 ± 24.5	198.3 ± 126.8
		0.11			10.5 ± 1.0	4.0 ± 0.8	119.8 ± 3.5	331.9 ± 30.4
		0.43			10.4 ± 1.0	4.3 ± 1.4	188.0 ± 11.6	229.3 ± 65.0
		0.48			8.7 ± 2.2	n.d.		60.9 ± 12.0
		0.62			14.6 ± 6.2	n.d.	48.8 ± 4.0	20.4 ± 17.3
		0.81			13.5 ± 6.9	n.d.	60.3 ± 6.6	n.d.
		1.17			24.4 ± 14.6	n.d.	78.5 ± 10.4	n.d.
		1.20			n.d.	n.d.	114.7 ± 14.1	n.d.
					10.8 ± 0.7	**4.0 ± 0.7**		
Average			102 ± 44	8 ± 18	11.5 ± 0.6	3.6 ± 0.4	120.3 ± 4.7	209.1 ± 19.7